JCTC Journal of Chemical Theory and Computation

Article

pubs.acs.org/JCTC

Nonadiabatic Ensemble Simulations of *cis*-Stilbene and *cis*-Azobenzene Photoisomerization

Amanda J. Neukirch,*[,†,‡] Logan C. Shamberger,[‡] Enrique Abad,[§] Barry J. Haycock,[‡] Hong Wang,[‡] José Ortega,[∥] Oleg V. Prezhdo,[†,⊥] and James P. Lewis*[,‡]

[†]Department of Physics and Astronomy, University of Rochester, Rochester, New York 14627, United States

[‡]Department of Physics and Astronomy, West Virginia University, Morgantown, West Virginia 26506-6315, United States

[§]Computational Biochemistry Group, Institute of Theoretical Chemistry, University of Stuttgart, 70569 Stuttgart, Germany

[∥]Departmento de Física Teórica de la Materia Condensada and Conensed Matter Physics Center (IFIMAC), Universidad Autónoma de Madrid, Madrid 28049, Spain

[⊥]Department of Chemistry, University of Rochester, Rochester, New York 14627, United States

ABSTRACT: Structurally, stilbene and azobenzene molecules exist in closed and open *cis* and *trans* forms, which are able to transform into each other under the influence of light (photoisomerization). To accurately simulate the photoisomerization processes, one must go beyond ground-state (Born−Oppenheimer) calculations and include nonadiabatic coupling between the electronic and vibrational states. We have successfully implemented nonadiabatic couplings and a surface-hopping algorithm within a density functional theory approach that utilizes local orbitals. We demonstrate the effectiveness of our approach by performing molecular dynamics simulations of the *cis*−*trans* photoisomerization in both azobenzene and stilbene upon excitation into the S_1 state. By generating an ensemble of trajectories, we can gather characteristic transformation times and quantum yields that we will discuss and compare with ultrafast spectroscopic experiments.

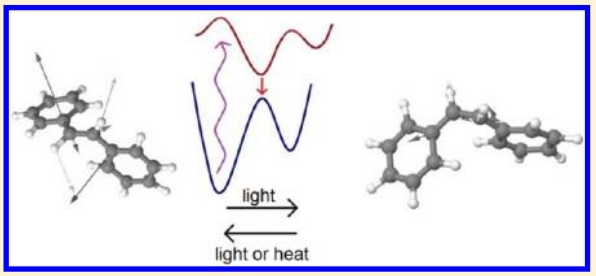

INTRODUCTION

Both stilbene and azobenzene can be interconverted between their *cis*- and *trans*-isomers by light of different wavelengths (Figure 1). Each isomer has distinct spectral and geometric properties that allow these molecules to serve as ideal model systems for molecular transducers in light-driven devices and optical switches.[1] The scientific community has invested considerable effort to harness the molecular motion of systems on the macroscopic scale. Applications range from optical storage devices,[2,3] regulating channels in the ligand-binding domain of proteins,[4] photo-orientation of liquid crystals,[5,6] control of peptide conformations,[7] modifying surface properties on oriented films,[8] and control of CO_2 adsorption in porous metal organic frameworks (MOF).[9]

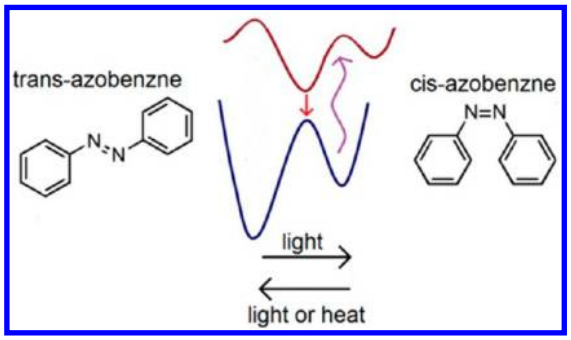

Figure 1. Simplified excitation and reaction schemes for azobenzene. Stilbene can be represented in a similar manor.

A detailed description of the photoisomerization process, especially in azobenzene, remains elusive, despite a plethora of novel applications and considerable theoretical and experimental studies. There are four possible pathways for isomerization in azobenzene: rotation, inversion, concerted inversion, and inversion-assisted rotation.[10−14] In the rotational pathway, the N═N π-bond breaks, allowing for free rotation around the N−N bond,[13] and the C−N═N−C dihedral angle changes, while the N═N−C angles remain fixed at ∼120°. In the inversion mechanism, the C−N═N−C angle remains fixed at 0°, but one of the N═N−C angles increases to 180°.[14] A linear transition state is produced in the concerted inversion mechanism when both N═N−C bond angles increase to 180°. Finally, in the inversion-assisted rotation mechanism, there are large changes in both the C−N═N−C angle and the N═N−C angles simultaneously. No barrier exists along the rotational pathway after excitation into the S_1 state. According to previous computational research, the conical intersection between the S_0 and S_1 states exists when the C−N═N−C dihedral angle is ∼90° and the N═N−C angle is ∼140°. These facts have

Received: November 13, 2013
Published: December 4, 2013

   dx.doi.org/10.1021/ct4009816 | *J. Chem. Theory Comput.* 2014, 10, 14−23

prompted the acceptance of rotation as the dominant mechanism with concerted inversion occurring under rotation-restricted conditions. Recent simulations have predicted isomerization of azobenzene through a pedal-like motion of the nitrogen atoms.[15−17]

It is well documented that electronically excited *trans*-stilbene undergoes relaxation via rotation about the ethylene bond and returns to the electronic ground state in either the *cis*- or *trans*-configuration with equal probability.[18] In *cis*-stilbene, a one-dimensional model focusing solely on rotation around the ethylene bond is insufficient to explain the processes that take place.[19] The ground state geometry of *cis*-stilbene is nonplanar due to steric repulsion; therefore, both photo isomerization to the *trans*-configuration and photocyclization to form 4a,4b-dihydrophenanthrene (DHP) are accessible from the *cis*-isomer of stilbene. Previous theoretical and experimental studies[20,21] have provided evidence that in addition to torsion phenyl rotation and pyramidalizaiton both play important roles in the isomerization process. Any study that hopes to reproduce the processes taking place, as well as experimental time scales and quantum yields, will have to allow for motion along each of these coordinates.

In both stilbene and azobenzene, the most efficient *cis*-to-*trans* photoconversion pathway proceeds via excitation into the first electronically excited state (450 nm n−π^*excitation in azobenzene and 270 nm $\pi-\pi^*$ excitation in stilbene),[10,22−24] followed by an ultrafast (hundreds of fs) decay through an S_1/S_0 conical intersection. The *cis*-conformation reacts faster than the *trans*-conformation for both systems.[25−35] Azobenzene is more efficient at isomerization compared to stilbene, as the quantum yield for the *cis*-to-*trans* conformational change is 40−69%[22,26,29,36−39] (depending on solvent) and 35%,[40] respectively. Stilbene will have 10% of its population end in the DHP configuration.

Harnessing the photoisomerization process and increasing its applicability to a variety of materials and systems will require a deeper theoretical understanding of the underlying mechanisms. Density functional theory (DFT) and molecular dynamics (MD) provides direct access to electronic and dynamic processes on the atomic scale and will semi-quantitatively ascertain the properties of materials. Unfortunately, a large majority of the current DFT-MD approaches utilize the Born−Oppenheimer approximation, where the system evolves in the electronic *ground* state. A more accurate depiction of the mechanisms in photoisomerization simulations requires a more complete theoretical methodology beyond the Born−Oppenheimer approximation.

In this work, we demonstrate that our previously implemented[41] nonadiabatic (NA) MD formalism appropriately simulates the photoisomerization process by allowing the nuclear motion to change the quantum state of the electronic subsystem. Our NAMD methodology uses the fewest switches surface-hopping (FSSH)[42] algorithm within an ab initio local orbital DFT framework. Here, we model the photoinduced isomerization of the *cis*-stilbene and *cis*-azobenzene in the S_1 state. Our method distinguishes between two distinct molecules, while simultaneously matching experimental results regarding quantum yields and relaxation times. Our ab initio approach allows for extended systems, molecules, and functional groups to be treated on equal footing and does not require parametrization for each new material. The efficiency of our local orbital density-functional theory code allows us to collect ensemble data large enough to identify the phonon modes that drive relaxation and isomerization. Knowledge of the active phonon modes, along with direct access to the nonadiabatic coupling vectors, provides insight into why quantum yields vary in different systems. Finally, our method is capable of simulating thousands of atoms at a time, allowing for future theoretical investigation of these small molecules incorporated in larger systems.

THEORETICAL AND COMUTATIONAL DETAILS

Historically, NAMD is simulated by one of two methods: Ehrenfest dynamics[43−46] and surface hopping.[42,47−53] In the Ehrenfest approach, the nuclei move classically on a single effective potential energy surface (PES) obtained by taking the average over all of the adiabatic states involved. Surface-hopping methods obtain the electronic occupations by averaging over an ensemble of initial conditions. At any given time, the nuclei in any given trajectory are evolving classically on a single PES. At each integration time step, a decision is made as to whether an electronic transition will occur according to the probabilistic "fewest switches" algorithm. After an electronic transition, energy is conserved by rescaling the nuclear velocities to account for the change in the system's electronic energy.[50,54−56] Surface-hopping methods are better equipped to handle systems where changes in the electronic populations sufficiently affect the nuclear motion,[57] as is the case with photo induced isomerization. Here, we use a time-dependent Kohn−Sham (TDKS) approach to perform NAMD.[48]

Our analysis uses a density functional theory approach, called FIREBALL, which is based on local orbitals within a nonlocal pseudopotential scheme.[58−60] FIREBALL is a molecular dynamics simulation technique that is based on a self-consistent functional,[61] where the basis set consists of numerical orbitals. The "fireball" orbitals, introduced by Sankey and Niklewski,[58] are acquired by producing slightly excited atom-in-the-box states that smoothly vanish outside of a predetermined radius, R_c. In this work, we use the Becke[62] exchange with the Lee−Yang−Parr correlation.[63] We have adopted double numerical sp^3 basis sets for *C* (cutoff radii of $R_c(s) = 4.4$ au and $R_c(p) = 4.8$ au) and *N* (curoff radii of $R_c(s) = 4.0$ au and $R_c(p) = 4.4$ au), whereas we use a minimal basis set for *H* (cutoff radius of $R_c(s) = 4.2$ au).

Within FIREBALL,[58−60] we explicitly calculate the nonadiabatic coupling vectors (NACV) "on the fly" during MD simulation.[41] In our implementation of NAMD simulations, atoms evolve along classical trajectories $\{\boldsymbol{R}_\alpha(t)\}$, but the interaction between the nuclear motion and electronic quantum state are explicitly accounted for through the inclusion the NACVs. We expand the time-dependent KS orbitals in terms of adiabatic eigenstates and evolve them using the TD Schrodinger equation in order to obtain the equation of motion for the expansion coefficients $a_i(t)$ (eq 1)

$$i\hbar\frac{\partial a_i(t)}{\partial t} = a_i(t)\varepsilon_i(\boldsymbol{R}) - i\hbar\sum_j a_j(t)\boldsymbol{d_{ij}}\cdot\boldsymbol{V} \tag{1}$$

The nonadiabatic coupling term represents the coupling between the classical motion of the nuclei and the electronic quantum state,

$$\boldsymbol{d_{ij}}\cdot\boldsymbol{V} \overset{\text{def}}{=} \sum_\alpha d_{ij}^\alpha \boldsymbol{V}_\alpha \tag{2}$$

dx.doi.org/10.1021/ct4009816 | J. Chem. Theory Comput. 2014, 10, 14−23

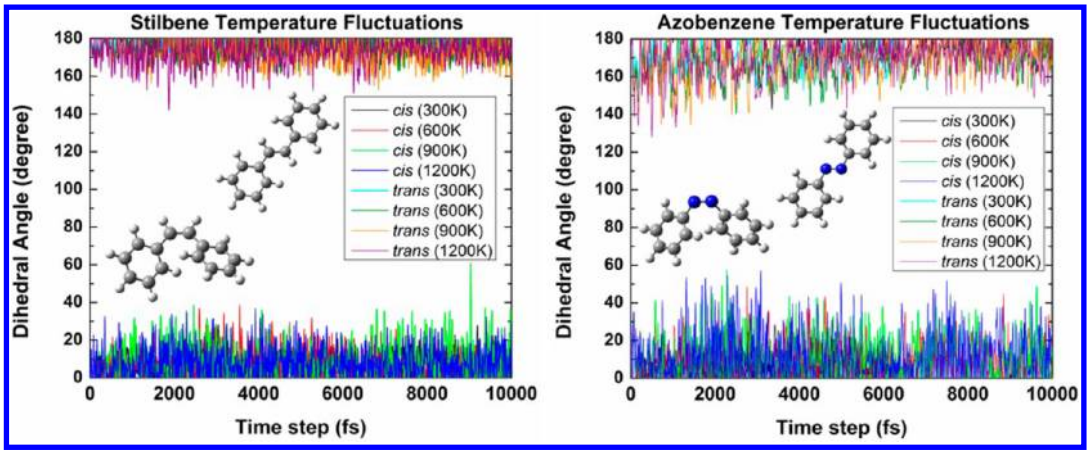

Figure 2. (Left) Plot of the dihedral angle around the C=C bond for both *cis*- and *trans*-stilbene from constant temperature ground-state molecular dynamics simulations. (Right) Plot of the dihedral angle around the N=N bond for both *cis*- and *trans*-azobenzene.

where $\boldsymbol{V}_\alpha = (\partial \boldsymbol{R}_\alpha/\partial t)$ is the atomic velocity; and α and $\boldsymbol{d}_{ij}$ are the nonadiabatic coupling vectors between the single particle KS states

$$\boldsymbol{d}_{ij}^{\alpha} \equiv \left\langle \psi_i \left| \frac{\partial \psi_j}{\partial \boldsymbol{R}_\alpha} \right\rangle \right. \tag{3}$$

We have implemented the FSSH algorithm proposed by Tully to obtain the correct statistical distribution of the state populations at all times.[42,47] The probability of a hop between states i and j within given time interval dt is

$$g_{ij} = \max\left(0, \frac{b_{ij}\Delta t}{|a_j(t)|^2}\right), \text{ where } b_{ij} = -2\mathrm{Re}[a_j^* a_k \boldsymbol{d}_{ij}\cdot\boldsymbol{V}] \tag{4}$$

The hopping probability depends explicitly on the nonadiabatic coupling defined in eqs 2 and 3. Setting the surface hopping probability to zero when g_{ij} is determined to be negative ensures that a hop from state i to state j occurs only if the occupation of state i decreases and the occupation of state j increases. The calculated probabilities are compared with a random number to determine an electronic transition. We impose energy conservation during electronic transitions by rescaling the nuclear velocities after an electronic transition takes place. Hops to higher energy electronic states are rejected if insufficient kinetic energy is present. Velocity rescaling and hop rejection ensures detailed balance between transitions up and down in energy.[64,65]

In the FIREBALL implementation the Hamiltonian matrix elements are calculated beforehand and stored in data tables. This a priori calculation of the system's interactions greatly speeds up MD simulations.[58−60] We have also developed an efficient algorithm for calculating the NACV's *on-the-fly* during a MD run.[41] The expression for $\boldsymbol{d}_{ij}^{\alpha}$, derived in ref 41,

$$\boldsymbol{d}_{ij}^{\alpha} = \frac{1}{\varepsilon_i - \varepsilon_j} \sum_{\mu\nu} c_{i\mu}^* c_{j\nu} \left[-\frac{\partial \langle \varphi_\mu | \hat{H}_{\mathrm{KS}} | \varphi_\nu \rangle}{\partial \boldsymbol{R}_\alpha} + \varepsilon_j \left\langle \frac{\partial \varphi_\mu}{\partial \boldsymbol{R}_\alpha} \middle| \varphi_\nu \right\rangle + \varepsilon_i \left\langle \varphi_\mu \middle| \frac{\partial \varphi_\nu}{\partial \boldsymbol{R}_\alpha} \right\rangle \right] \tag{5}$$

includes only the eigenvalues, ε_i, the expansion coefficients of the single-particle states in the local orbital basis $c_{i\mu}$, and information already stored in the precomputed data tables. In eq 5, the NACVs are calculated using the Kohn−Sham eigenvalues, ε_i, ε_j, the expansion coefficients $c_{i\mu}$, and the derivatives $(\partial\langle\phi_\mu|\hat{H}_{\mathrm{KS}}|\phi_\nu\rangle/\partial\boldsymbol{R}_\alpha)$, $\langle(\partial\phi_\mu/\partial\boldsymbol{R}_\alpha)|\phi_\nu\rangle$, and $\langle\phi_\mu|(\partial\phi_\nu/\partial\boldsymbol{R}_\alpha)\rangle$. Hence, all of the NACVs are efficiently evaluated because all of the derivatives that appear in this expression are obtained from precomputed information.

We initially optimize the geometry of each molecule (stilbene and azobenzene) so that it is in its lowest energy *cis*-configuration. The system evolves at 300 K for 6.5 ps using ground-state MD using a canonical ensemble.[66] Random coordinates are selected from the MD trajectory with an automated python script, and we use these random configurations as the initial coordinates for our MD simulations with electronic transitions. The initial velocities are generated randomly such that the system is 300 K and has no total translational or angular momentum. In this study, we analyze the results from 400 NAMD trajectories starting from *cis*-azobenzene (or *cis*-stilbene) beginning in the S_1 state and evolving in the microcanoical ensemble for up to 750 fs. The S_1 state is defined using restricted self-consistent DFT calculations with one electron in the Kohn−Sham LUMO level and one hole in the HOMO level. The nuclear time step was 0.25 fs, and the electronic time step was 0.0025 fs during these simulations. Over 99% of the trajectories had relaxed to the ground state (S_0) within the 750 fs. We evaluate the *cis*- or *trans*-conformations by monitoring the central dihedral angle after relaxation into the ground state. If the angle evolved to >155° after electronic relaxation, then we counted this conformation as *trans*. If the angle evolved to <25° after electronic relaxation, then we counted this conformation as *cis*.

RESULTS AND DISCUSSION

We performed ground state MD simulations for both *cis*- and *trans*-stilbene (left panel, Figure 2) and azobenzene (right panel, Figure 2) at different fixed temperatures (300, 600, 900, and 1200 K). Both stilbene and azobenzene are capable of thermally converting from the *cis*-to-*trans* configuration via thermal fluctuations.[67] The lifetime of the *cis* conformation ranges from milliseconds to hours depending on the derivative involved and local environment.[68] On the ps time scale, we do not observe any instances of thermal conversion in either molecular system starting from either configuration.

In order to simulate photoexcitation into the S_1 state, we remove an electron from the HOMO and place it in the

dx.doi.org/10.1021/ct4009816 | J. Chem. Theory Comput. 2014, 10, 14−23

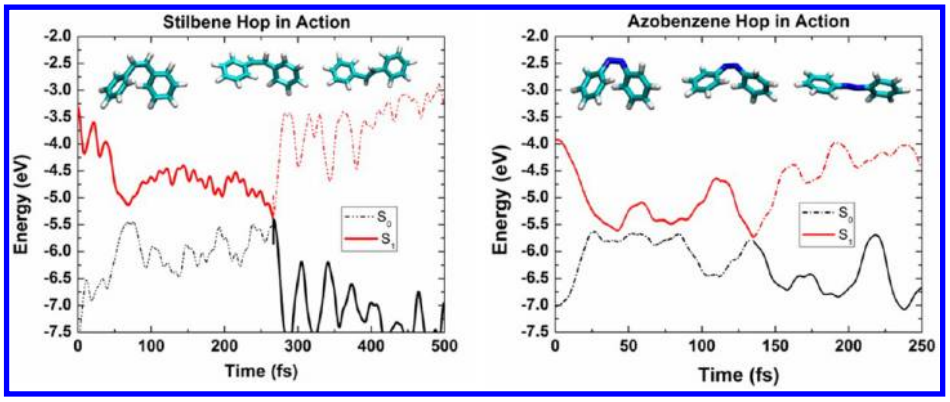

Figure 3. Evolution of HOMO and LUMO energies as the system relaxes from the S_1 to S_0 state for stilbene (left) and azobenzene (right).

LUMO. Figure 3 shows the evolution of the HOMO and LUMO energy levels along a single trajectory in stilbene (left) and azobenzene (right); the bold lines record in which state the initially excited electron is located. After excitation, the system evolves in the excited state until the HOMO and LUMO approach near degeneracy (conical intersection). The electron then relaxes into the HOMO (probabilistic hop, see eq 4), and then the system evolves on the S_0 state. The plotted stilbene trajectory indicates that there is almost a conical intersection at around 90 fs. However, a hop does not take place, and the system continues to evolve in the S_1 state. The system returns to the ground state, S_0, when a hop occurs at 265 fs, and the HOMO−LUMO band gap proceeds to rapidly increase. This trajectory of stilbene ends in the *trans*-configuration. Along the top of the figure is the pictorial evolution of the atomic coordinates. The system starts in the *cis*-configuration. Near the conical intersection, the rotation about the C═C bond is initiated, and by the end of the trajectory, the system is in the *trans*-configuration. In the selected azobenzene trajectory, the HOMO and LUMO approach near degeneracy very quickly (∼ 25 fs), but a switch does not occur until 135 fs. Despite the subtle differences presented in these two trajectories, it is important to not assume trends by examining the results of two individual trajectories.

In Figure 4, we plot the HOMO occupation and dihedral angle as a function of time for one trajectory that remains in the *cis*-configuration and one trajectory that photoisomerizes into the *trans*-configuration for stilbene and azobenzene. In all four cases presented, the relaxation to the ground state happens within 200 fs, and the dihedral angle quickly transforms from 0° to the conical intersection at 90°. In the azobenzene trajectory that ends in the *trans*-configuration, the system briefly relaxes into the ground state but then re-excites before the system exits the conical intersection. Unsuccessful relaxation events take place in both stilbene and azobenzene in trajectories that end in either isomer. For the purpose of this study, we consider the time of transition to be the time when the system relaxes electronically ($S_1 \rightarrow S_0$) and remains in the S_0 state and remains relaxed until the system reaches the *trans* (>155°) or *cis* (<25°) configuration. In the case of the example illustrated in the bottom panel of Figure 4, the relaxation time is 205 fs.

We are only able to get reliable experimental parameters by looking at ensemble averages. Figure 5 shows the distribution of the transistion (or relaxation) times for the stilbene (left) and azobenzene (right) ensembles. The average relaxation time for stilbene (left panel) is 195 fs. There are actually two peaks in the relaxation times: one at 40 fs and one at 160 fs. The

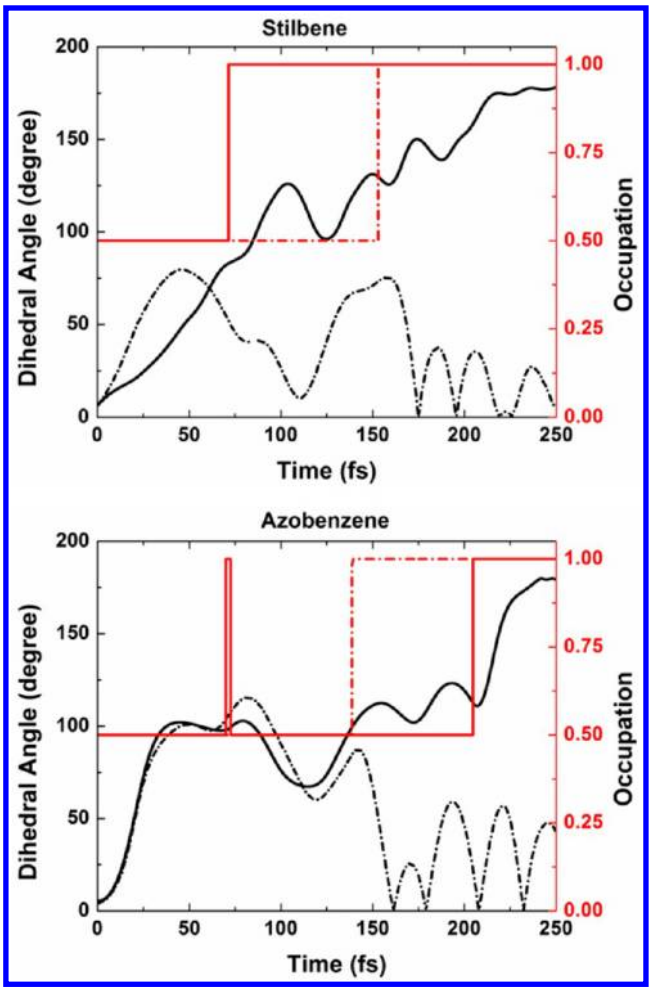

Figure 4. Plot of the dihedral angle (black) and HOMO occupation (red) for two trajectories in stilbene (top) and azobenzene (bottom). One of the trajectories remains in the *cis*-stilbene configuration (dashed line), while the other leads to *trans*-stilbene isomerization (solid line).

relaxation times extend into longer times, but the population in the excited state decays rapidly. The temporal distribution is similar for both *cis* and *trans*-trajectories. Our 195 fs lifetime is consistent with reported experimental lifetimes that range anywhere between 160 and 320 fs.[32−35] We found a quantum yield of 34%, in agreement with experimental results of 35%.[40] We did not observe any trajectories that ended up in the DHP configuration. However, DHP formation takes place on a time

dx.doi.org/10.1021/ct4009816 | J. Chem. Theory Comput. 2014, 10, 14−23

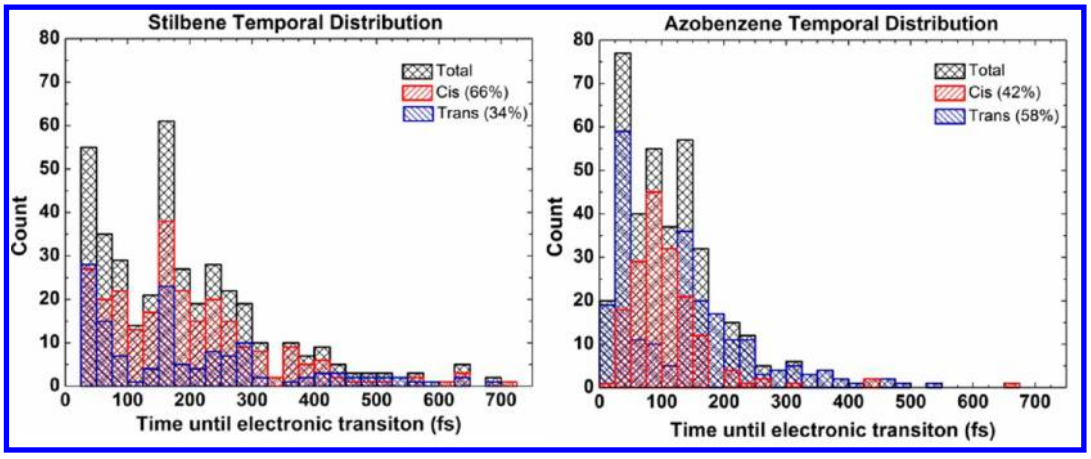

Figure 5. Distribution of the transistion times for the *cis* → *trans* photoisomerization of (left) stilbene and (right) azobenzene. Black cross bars represent all trajectories. Red slashed lines represent transitions that end in *cis*-configuration. Blue slashed lines represent transitions that end in the *trans*-configuration.

scale of a couple of picoseconds, and our trajectories are only propagated for 750 fs.[18]

The average relaxation time in azobenzene is 121 fs (right panel), which is significantly faster than stilbene. This relaxation time is also in good agreement with previous experimental and theoretical results ranging from 60 to 200 fs.[25−31] In azobenzene, we see a difference in the average relaxation times between systems that culminate in the *trans* (129 fs) or *cis* (103 fs) configuration. We observe two peaks at around 40 and 140 fs in the distribution of trajectories that finish in the *trans*-configuration. There is a single peak around 90 fs in the distribution of trajectories that finish in the *cis*-configuration. Other groups have observed multiple peaks at similar time scales in the overall relaxation distribution.[29] We found the quantum yield for azobenzene to be 58%, which is significantly higher than what we observed for stilbene. This quantum yield is in agreement with both experimental and theoretical results, which range from 40% to 69%.[22,29,36−39]

We also show the distribution of the dihedral angle at the time of the $S_1 \rightarrow S_0$ electronic transition in Figure 6. In both stilbene and azobenzene, the distribution peaks between 80° and 90°. The average dihedral angle in stilbene (top panel) is 81°, and the average angle in azobenzene (bottom panel) is 94°. An investigation using the complete active space self-consistent field and multi-reference perturbation theory found that stilbene had a conical intersection at 85°.[19] Several studies have found that the conical intersection in azobenzene is approximately 96°.[29,36] Stilbene and azobenzene are more likely to remain in the *cis*-configuration if the system undergoes electronic relaxation into the ground state when the dihedral angle is less than 80°. Both molecular systems are more likely to isomerize into the *trans*-conformation if the electronic transition into the ground state occurs when the dihedral angle is greater than 100°. The azobenzene trajectories have a narrower angular distribution compared to stilbene, suggesting that azobenzene may have a narrower conical intersection. The biggest difference between the two systems is that, in our investigation, stilbene has more trajectories that undergo an electronic transition when the dihedral angle is less than 60°, while azobenzene had more trajectories that undergo an electronic transition when the dihedral angle is greater than 120°. Electronically excited azobenzene relaxes faster than electronically excited stilbene (Figure 5) and is more likely to undergo electronic transitions at larger dihedral angles. Therefore, the S_1 state potential energy surface along the dihedral angle reaction coordinate is very likely steeper for

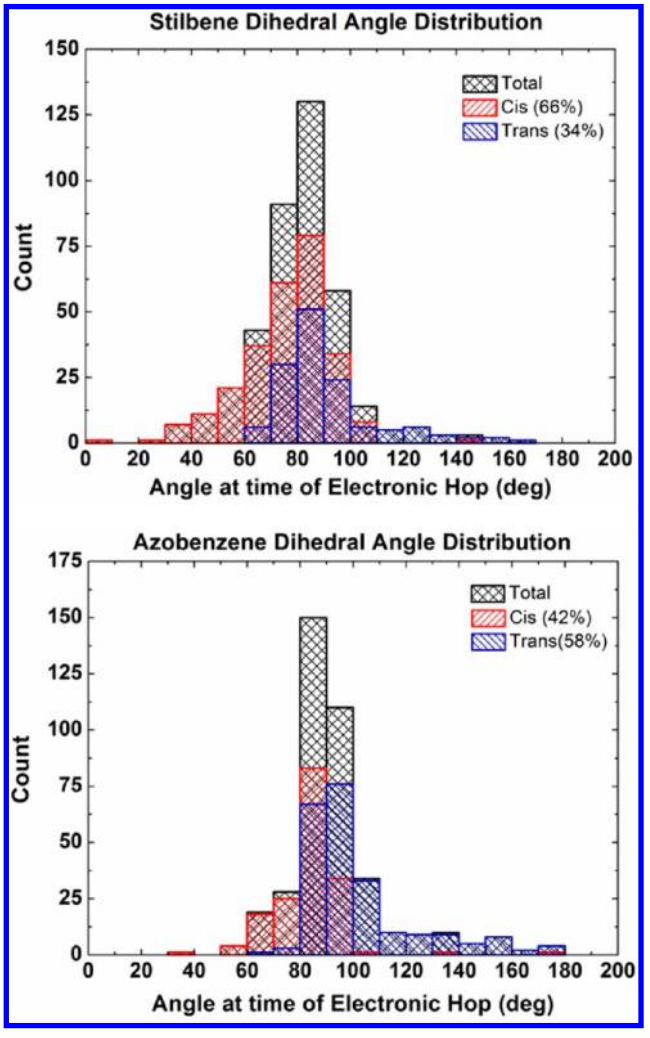

Figure 6. Distribution of the C−C═C−C (stilbene) and C−N═N−C (azobenzene) dihedral angle at the time the electronic hop took place. Trajectories yielding the *trans*-configuration are shown in blue, while those yielding the *cis*-configuration are shown in red.

dx.doi.org/10.1021/ct4009816 | J. Chem. Theory Comput. 2014, 10, 14−23

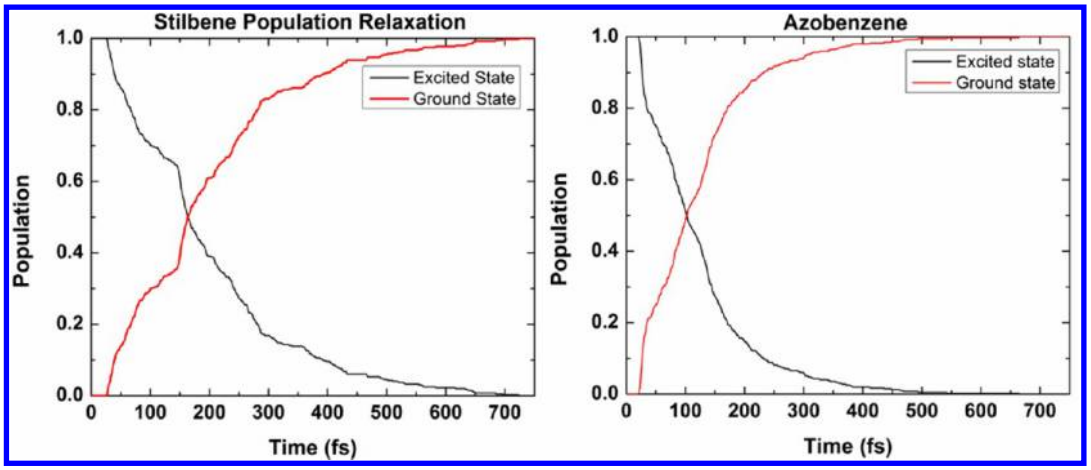

Figure 7. Left panel is the evolution of the ground and excited state populations for stilbene. Right panel is the evolution of the ground and excited state populations for azobenzene.

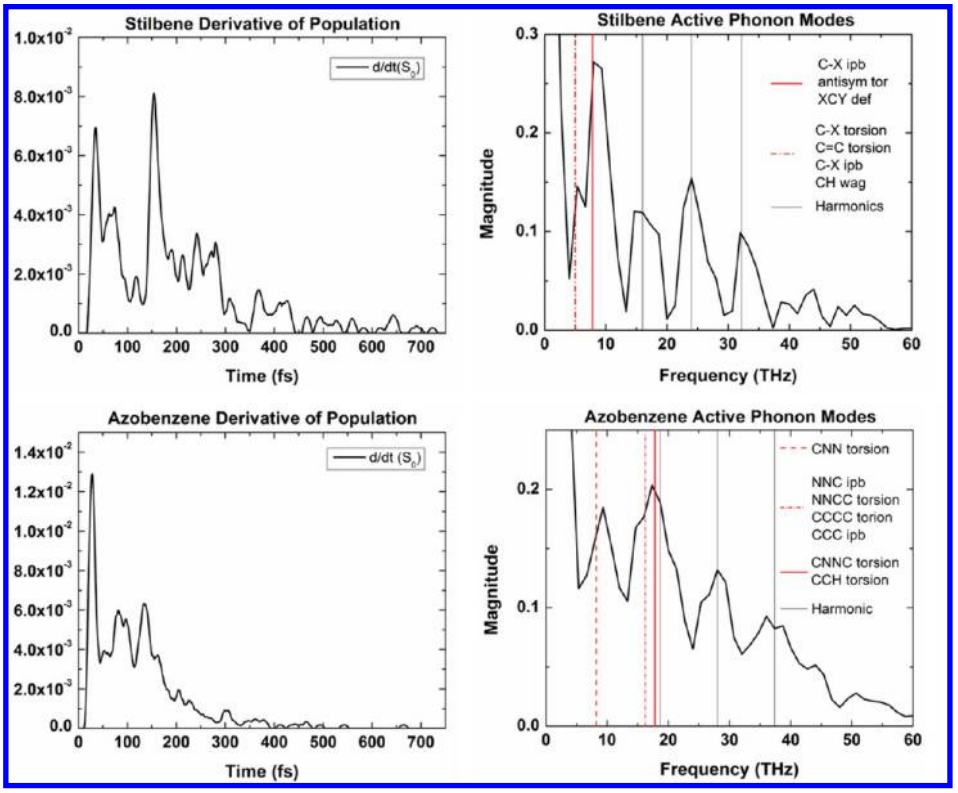

Figure 8. (Left) Top panel is the derivative of the population of S_0 state for stilbene. Bottom panel is the derivative of the S_0 population for azobenzene. (Right) Fourier transforms of the derivatives of the S_0 population in stilbene (top) and azobenzene (bottom).

azobenzene than it is for stilbene (Figure 1), offering a potential explanation as to why azobenzene has a higher *cis*-to-*trans* quantum yield compared to stilbene.

Another way of representing the relaxation dynamics is to track the populations in the ground and excited state. In Figure 7 , we track the percentage of trajectories that have undergone an electronic transition into the ground state that lead to a definite *cis*- or *trans*-configuration at each time step. Once a trajectory returned to the ground state and definitively went into the *cis*- or *trans*-configuration, we no longer followed its population fluctuations. Figure 7 illustrates that the relaxation of azobenzene is smoother compared to the relaxation of stilbene. In stilbene, the relaxation curve has a few plateaus in the population events.

We determine the phonon modes involved in relaxation and isomerization by taking the Fourier transform of the derivative of the population in the S_0 state (ground state).[69] The left side of Figure 8 shows the derivatives of the S_0 populations for both of the systems (top panel stilbene; bottom panel azobenzene). Oscillatory patterns, similar to what were found for both stilbene and azobenzene in the hopping time distributions (Figure 5), were found in the derivative graphs. In stilbene, this oscillatory pattern is manifested in peaks at 35 and 155 fs, and in azobenzene, we observe three distinct peaks at 30, 80, and 135 fs.

The right side of Figure 8 shows the Fourier transforms of the derivatives of the S_0 population in stilbene (top) and azobenzene (bottom). The peaks at 0 THz in both systems

dx.doi.org/10.1021/ct4009816 | J. Chem. Theory Comput. 2014, 10, 14−23

originate from artifacts inherent to Fourier transforms. In the frequency domain, stilbene has a distinct peak at around 267 cm^{-1} (8 THz) and a small peak at around 178 cm^{-1} (5.33 THz). Raman spectroscopy experiments have identified a mode at 166 cm^{-1} (5 THz) in *cis*-stilbene that receives substantial contributions from phenyl twisting and ethylenic torsion. They have also identified a mode in stilbene at 261 cm^{-1} (7.83 THz) associated with ethylenic torsion and in-plane bending.[70−75] We find azobenzene exhibits peaks in the frequency domain at around 312 cm^{-1} (9.35 THz), 534 cm^{-1} (16 THz), and 580 cm^{-1} (17.36 THz). Experimentalists have identified a mode at 600 cm^{-1} (18 THz) associated with torsion of the CNNC dihedral angle, a mode that is essential in *cis*-to-*trans* isomerization.[76] Experimental peaks associated with CCNN torsion at 275 cm^{-1} (8.25 THz) and 542 cm^{-1} (16.25 THz) match the other peaks found in our frequency analysis. From our results, we find that azobenzene couples most strongly to the mode at 17.36 THz associated with torsion of the CNNC dihedral angle, while stilbene couples most strongly to the mode at 8 THz associated with asymmetric torsion and in-plane bending. A mode associated with torsion of the CNNC dihedral is going to be more efficient at isomerization compared to a mode associated with asymmetric torsion and in-plane bending, offering an explanation as to why azobenzene has a higher quantum yield.

In both molecular systems, the dihedral angle increases from 0° to 90° and then either decreases down to 0° or increases up to 180° during the relaxation and isomerization process after the electronic transition. This process suggests a rotational pathway. By studying the projections of the nonadiabatic coupling vectors onto individual atoms in the molecular systems, we elucidate more information about the pathway toward relaxation and isomerization. In order to do this, we chose and examined 10 representative trajectories with relaxation times and dihedral angles similar to the ensemble distributions that ended up in each conformation for each molecular system. In both systems, we find that the center atoms contribute the most to the nonadiabatic coupling terms; hence, they are the more influential atoms in this process.

Table 1 illustrates the average magnitude of the nonadiabatic coupling vector, $|d_{ij}|$, and absolute value of the nonadiabatic coupling terms, $|\boldsymbol{d}_{ij}\cdot\boldsymbol{V}|$, taken from the influential central atoms in stilbene. For transitions that end in the *cis*-configuration, our data shows that the magnitude of the nonadiabatic coupling vector for each of the influential central atoms is about the same for each examined trajectory. Differences in the nonadiabatic coupling terms exist because the center hydrogen atoms possess a greater velocity. Our data also shows that the coupling terms and vectors are greater for trajectories that end in the *trans*-configuration. The magnitude of the nonadiabatic coupling vectors and the absolute value of the entire nonadiabatic coupling constant acquire the largest contributions from C1 an C2, as well as the hydrogen atoms in the center H15 an H16 (top panel, Figure 9).

Table 1. Ensemble Averages for Values of Modulus of Projection on Some Atoms (C1, C2, C3, C4, H15, and H16; Figure 9) of the Nonadiabatic Coupling Vectors and Absolute Value of Nonadiabatic Coupling Term between HOMO and LUMO at the Time Instantaneously before the Electronic Transition into the Ground State in Stilbene

	cis		*trans*	
	$\lvert d_{ij}\rvert$ (A^{-1})	$\lvert\boldsymbol{d}_{ij}\cdot\boldsymbol{V}\rvert$ (THz)	$\lvert d_{ij}\rvert$ (A^{-1})	$\lvert\boldsymbol{d}_{ij}\cdot\boldsymbol{V}\rvert$ (THz)
C1	7.02	21	15.06	135
C2	8.25	18	20.42	75
C3	5.36	28	7.82	52
C4	5.60	21	6.66	56
H15	6.00	84	12.04	380
H16	6.15	108	12.15	162

We elucidate more by considering the directions of the couplings vectors immediately preceding an electronic transition from a single representative trajectory that ends in each conformation. Figure 9 shows the optimized structure with the central atoms labeled (top center); the atomic nonadiabatic coupling vectors are superimposed on the atoms for the case of a trajectory that ends in the *cis*-configuration (bottom right) and *trans* configuration (bottom left) for stilbene. In the trajectory that ends in the *trans*-configuration, we see that the NACVs are the largest for atoms C1, C2, H15, and H16. The NACVs for atoms C3 and C4 are much smaller, supporting that the stilbene isomerization pathway is rotation around the double ethylenic bond.[18] In the unreactive trajectory, the NACVs are of the same order of magnitude for each of the center atoms.

In azobenzene, the magnitude of the averaged nonadiabatic coupling vectors from the chosen trajectories is similar for all central atoms in both reactive and unreactive trajectories (Table 2). There is a large difference manifested in the nonadiabatic coupling constant, $|\boldsymbol{d}_{ij}\cdot\boldsymbol{V}|$, where in reactive trajectories the central nitrogen atoms become dominant. The large coupling constants are an indication that the velocities are nearly parallel to the coupling vectors. Finally, in both stilbene and azobenzene, there is an asymmetric contribution to the total coupling from each symmetric half of the center atoms in reactive trajectories. This asymmetry could explain the chirality of the system as other groups have reported.[29]

Looking at Figure 10, we see that in the *trans* case (bottom left) the nitrogen atoms possess the largest NACVs, while atoms in the phenyl ring have smaller NACVs, confirming the pedal-like rotational motion previously predicted.[15−17] The *cis* trajectory (bottom right) has similar and smaller coupling vectors for all of the center atoms.

CONCLUSION

In conclusion, a combination of efficient local orbital density functional theory with the fewest switches surface-hopping algorithm has allowed us to run a large number of isomerization events in order to perform a statistical analysis that compares well with experiments. This study focused on the *cis*−*trans* photoisomerization of stilbene and azobenzene, which were excited into the S_1 state. We were able to capture accurate quantum yields and excited state lifetimes as well as an accurate conical intersection at 90°. The dihedral angle at the time of electronic transition is an early indicator of what the resulting conformation will be. Both molecular electronic systems couple to phonon modes that are dominant in the isomerization process. Knowledge of the active phonon modes and direct access to the nonadiabatic coupling vectors provides insight into why quantum yields may vary in different systems. We obtain detailed information on the isomerization mechanism by considering the nonadiabatic coupling vectors. Stilbene undergoes isomerization via rotation about the double ethylenic bond. In azobenzene, the central N═N initializes the

dx.doi.org/10.1021/ct4009816 | J. Chem. Theory Comput. 2014, 10, 14−23

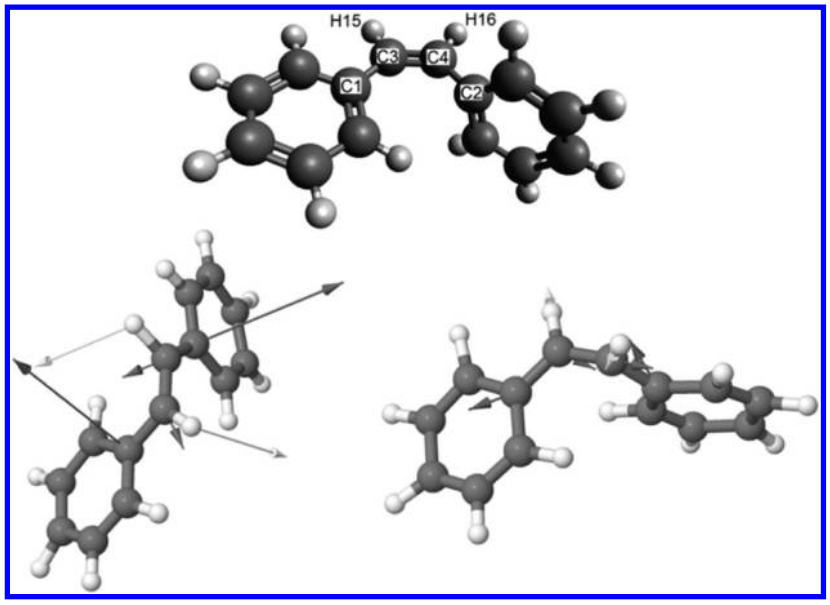

Figure 9. Top panel shows the stilbene molecule in the *cis*-conformation with labels on atoms defined according to Table 1. Bottom left panel shows the dominant nonadiabatic coupling vectors for a representative trajectory that ends in the *trans*-configuration. Bottom right panel shows the dominant coupling vectors for a representative trajectory that ends in the *cis*-configuration.

Table 2. Ensemble Averages for Values of Modulus of Projection on Some Atoms (C3, N12, N13, C14; Figure 10) of the Nonadiabatic Coupling Vectors and Absolute Value of Nonadiabatic Coupling Term between HOMO and LUMO at Time Preceding Electronic Transition into the Ground State in Azobenzene

	cis		*trans*	
	$\lvert d_{ij}\rvert$ (A^{-1})	$\lvert \boldsymbol{d}_{ij}\cdot\boldsymbol{V}\rvert$ (THz)	$\lvert d_{ij}\rvert$ (A^{-1})	$\lvert \boldsymbol{d}_{ij}\cdot\boldsymbol{V}\rvert$ (THz)
C3	6.16	46.56	7.33	33.4
C14	6.73	58.7	7.28	33.8
N13	8.40	54.8	9.94	151
N12	9.70	59.64	10.44	176

isomerization process through a pedal-like motion followed by the phenyl groups. The method we use is very general and can be applied to photoisomerization studies of most systems. Our parallel molecular dynamics code, FIREBALL, is capable of studying systems up to thousands of atoms in size, allowing for these photoswitchable molecules to be incorporated in extended structures with practical applications.

AUTHOR INFORMATION

Corresponding Authors

*E-mail: ajneuk@pas.rochester.edu (A.J.N.).
*E-mail: james.lewis@mail.wvu.edu (J.P.L.).

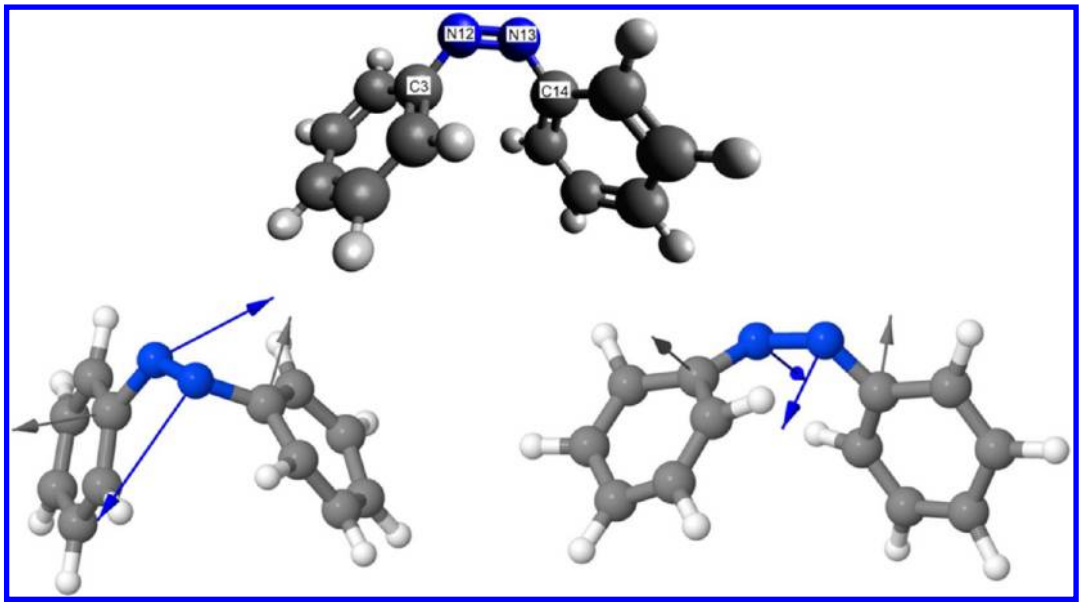

Figure 10. Top panel shows the azobenzene molecule in the *cis*-conformation and labels the atoms discussed in Table 2. Bottom left panel shows the dominant nonadiabatic coupling vectors for a representative trajectory that ends in the *trans*-configuration. Bottom right panel shows the dominant coupling vectors for a representative trajectory that ends in the *cis*-configuration.

Author Contributions

The manuscript was written through contributions of all authors. All authors have given approval to the final version of the manuscript.

Notes

The authors declare no competing financial interest.

■ ACKNOWLEDGMENTS

This work was partially supported by the Spanish Ministerio de Economía y Competitividad (Contract No. FIS2010-16046), Comunidad de Madrid (Contract No. S2009/MAT-1467), Office of Science, Basic Energy Sciences in the U.S. Department of Energy (Grant No. DEFG02-10ER16164 and Grant No. DE-SC0006527), and National Science Foundation (Grant No. CHE-1300118). J.O. gratefully acknowledges support from the Spanish Ministerio de Ciencia e Innovación (PR2008-0027). E.A. gratefully acknowledges financial support by the Consejería de Educación de la Comunidad de Madrid and Fondo Social Europeo.

■ REFERENCES

(1) Rau, H. *Photochromism: Molecules and Systems*; Durr, H., Bouas-Laurent, H., Eds.; Elsevier Science: Amsterdam, The Netherlands, 2003; p 1218.
(2) Ikeda, T.; Tsutsumi, O. *Science* **1995**, *268*, 1873−1875.
(3) Berg, R. H.; Hvilsted, S.; Ramanujam, P. S. *Nature* **1996**, *383*, 505−508.
(4) Volgraf, M.; Gorostiza, P.; Numano, R.; Kramer, R. H.; Isacoff, E. Y.; Trauner, D. *Nat. Chem. Bio.* **2006**, *2*, 47−52.
(5) Choi, H. J.; Jeong, K.-U.; Chien, L.-C.; Lee, M.-H. *J. Mater. Chem.* **2009**, *19*, 7124.
(6) Böckmann, M.; Peter, C.; Site, L. D.; Doltsinis, N. L.; Kremer, K.; Marx, D. *J. Chem. Theory Comput.* **2007**, *3*, 1789−1802.
(7) Renner, C.; Moroder, L. *Chembiochem* **2006**, *7*, 868−878.
(8) Pace, G.; Ferri, V.; Grave, C.; Elbing, M.; Von Hänisch, C.; Zharnikov, M.; Mayor, M.; Rampi, M. A.; Samorì, P. *Proc. Natl. Acad. Sci. U.S.A.* **2007**, *104*, 9937−9942.
(9) Park, J.; Yuan, D.; Pham, K. T.; Li, J.-R.; Yakovenko, A.; Zhou, H.-C. *J. Am. Chem. Soc.* **2012**, *134*, 99−102.
(10) Bandara, H. M. D.; Burdette, S. C. *Chem. Soc. Rev.* **2012**, *41*, 1809−1825.
(11) Crecca, C. R.; Roitberg, A. E. *J. Phys. Chem. A* **2006**, *110*, 8188−8203.
(12) Rau, H.; Luddecke, E. *J. Am. Chem. Soc.* **1982**, *104*, 1616−1620.
(13) Magee, J. L.; Shand, W.; Eyring, H. *J. Am. Chem. Soc.* **1941**, 677−688.
(14) Curtin, D. Y.; Grubbs, E. J.; Mccarty, C. G. *J. Am. Chem. Soc.* **1966**, *530*, 2775−2786.
(15) Böckmann, M.; Doltsinis, N. L.; Marx, D. *Phys. Rev. E* **2008**, *78*, 036101.
(16) Böckmann, M.; Doltsinis, N. L.; Marx, D. *J. Phys. Chem. A* **2010**, *114*, 745−754.
(17) Böckmann, M.; Marx, D.; Peter, C.; Site, L. D.; Kremer, K.; Doltsinis, N. L. *Phys. Chem. Chem. Phys.* **2011**, *13*, 7604−7621.
(18) Repinec, S. T.; Sension, R. J.; Szarka, A. Z.; Hochstrasser, R. M. *J. Phys. Chem.* **1991**, *95*, 10380−10385.
(19) Quenneville, J.; Martı, T. J. *J. Phys. Chem. A* **2003**, *107*, 829−837.
(20) Frederick, J. H.; Penn, J. H.; Virginia, W. *J. Phys. Chem.* **1991**, *95*, 2845−2858.
(21) Rodier, J.-M.; Myers, A. B. *J. Am. Chem. Soc.* **1993**, *115*, 10791−10795.
(22) Bortolus, P.; Monti, S. *J. Phys. Chem.* **1979**, *83*, 648−652.
(23) Nakamura, T.; Takeuchi, S.; Taketsugu, T.; Tahara, T. *Phys. Chem. Chem. Phys.* **2012**, *14*, 6225−6232.
(24) Rice, J. K.; Baronavski, A. P. *J. Phys. Chem.* **1992**, *96*, 3359−3366.
(25) Cattaneo, P.; Persico, M. *Phys. Chem. Chem. Phys.* **1999**, *1*, 4739−4743.
(26) Toniolo, A.; Ciminelli, C.; Persico, M.; Martínez, T. J. *J. Chem. Phys.* **2005**, *123*, 234308.
(27) Ootani, Y.; Satoh, K.; Nakayama, A.; Noro, T.; Taketsugu, T. *J. Chem. Phys.* **2009**, *131*, 194306.
(28) Pederzoli, M.; Pittner, J.; Barbatti, M.; Lischka, H. *J. Phys. Chem. A* **2011**, *115*, 11136−11143.
(29) Weingart, O.; Lan, Z.; Koslowski, A.; Thiel, W. *J. Phys. Chem. Lett.* **2011**, *2*, 1506−1509.
(30) Nagele, T.; Hoche, R.; Zinth, W.; Wachtveitl, J. *Chem. Phys. Lett.* **1997**, *272*, 489−495.
(31) Satzger, H.; Spörlein, S.; Root, C.; Wachtveitl, J.; Zinth, W.; Gilch, P. *Chem. Phys. Lett.* **2003**, *372*, 216−223.
(32) Fuß, W.; Kosmidis, C.; Schmid, W. .; Trushin, S. . *Chem. Phys. Lett.* **2004**, *385*, 423−430.
(33) Pedersen, S.; Bañares, L.; Zewail, A. H. *J. Chem. Phys.* **1992**, *97*, 8801.
(34) Baumert, T.; Frohnmeyer, T.; Kiefer, B.; Niklaus, P.; Strehle, M.; Gerber, G.; Zewail, A. H. *App. Phys. B* **2001**, *72*, 105−108.
(35) Greene, B. I.; Farrow, R. C. *J. Chem. Phys.* **1983**, *78*, 3336.
(36) Ciminelli, C.; Granucci, G.; Persico, M. *Chemistry (Weinheim an der Bergstrasse, Germany)* **2004**, *10*, 2327−2341.
(37) Zimmerman, G.; Chow, L.-Y.; Paik, U.-J. *J. Am. Chem. Soc.* **1958**, *80*, 3528−3531.
(38) Gegiou, D.; Muszkat, K. A.; Fischer, E. *J. Am. Chem. Soc.* **1968**, *90*, 12−18.
(39) Siampiringue, N.; Guyot, G.; Monti, S.; Bortolus, P. *J. Photochem.* **1987**, *37*, 185−188.
(40) Petek, H.; Yoshihara, K.; Fujiwara, Y.; Lin, Z.; Penn, J. H.; Frederick, J. H. *J. Phys. Chem.* **1990**, *94*, 7539−7543.
(41) Abad, E.; Lewis, J. P.; Zobač, V.; Hapala, P.; Jelínek, P.; Ortega, J. *J. Chem. Phys.* **2013**, *138*, 154106.
(42) Tully, J. C. *J. Chem. Phys.* **1990**, *93*, 1061.
(43) Isborn, C. M.; Li, X.; Tully, J. C. *J. Chem. Phys.* **2007**, *126*, 134307.
(44) Castro, A.; Isla, M.; Martínez, J. I.; Alonso, J. A. *Chem. Phys.* **2012**, *399*, 130−134.
(45) Meng, S.; Kaxiras, E. *J. Chem. Phys.* **2008**, *129*, 054110.
(46) Andrade, X.; Castro, A.; Zueco, D.; Alonso, J. L.; Echenique, P.; Falceto, F.; Rubio, A. *J. Chem. Theory Comput.* **2009**, *5*, 728−742.
(47) Hammes-Schiffer, S.; Tully, J. C. *J. Chem. Phys.* **1994**, *101*, 4657.
(48) Craig, C.; Duncan, W.; Prezhdo, O. *Phys. Rev. Lett.* **2005**, *95*, 163001.
(49) Doltsinis, N.; Marx, D. *Phys. Rev. Lett.* **2002**, *88*, 166402.
(50) Tapavicza, E.; Tavernelli, I.; Rothlisberger, U. *Phys. Rev. Lett.* **2007**, *98*, 023001.
(51) Tully, J. C. *J. Chem. Phys.* **1971**, *55*, 562.
(52) Herman, M. F. *J. Chem. Phys.* **1984**, *81*, 754.
(53) Kazaryan, A.; Lan, Z.; Sch, L. V; Thiel, W.; Filatov, M. *J. Chem. Theory Comput.* **2011**, *7*, 2189−2199.
(54) Coker, D. F.; Xiao, L. *J. Chem. Phys.* **1995**, *102*, 496.
(55) Prezhdo, O. V.; Rossky, P. J. *J. Chem. Phys.* **1997**, *107*, 825.
(56) Tavernelli, I.; Tapavicza, E.; Rothlisberger, U. *J. Mol. Struc: THEOCHEM* **2009**, *914*, 22−29.
(57) Horsfield, A. P.; Bowler, D. R.; Ness, H.; Sánchez, C. G.; Todorov, T. N.; Fisher, A. J. *Rep. Prog. Phys.* **2006**, *69*, 1195−1234.
(58) Sankey, O. F.; Niklewski, D. J. *Phys. Rev. B* **1989**, *40*, 3979.
(59) Lewis, J. P.; Jelínek, P.; Ortega, J.; Demkov, A. A.; Trabada, D. G.; Haycock, B.; Wang, H.; Adams, G.; Tomfohr, J. K.; Abad, E.; Wang, H.; Drabold, D. A. *Phys. Status Solidi B* **2011**, *248*, 1989−2007.
(60) Jelínek, P.; Wang, H.; Lewis, J.; Sankey, O.; Ortega, J. *Phys. Rev. B* **2005**, *71*, 235101.
(61) Demkov, A.; Ortega, J.; Sankey, O.; Grumbach, M. *Phys. Rev. B* **1995**, *52*, 1618−1630.
(62) Becke, A. . *Phys. Rev. A* **1988**, *38*, 3098−3100.
(63) Lee, C.; Yang, W.; Parr, R. G. *Phys. Rev. B* **1988**, *37*, 785−789.
(64) Parandekar, P. V; Tully, J. C. *J. Chem. Phys.* **2005**, *122*, 094102.

(65) Parandekar, P. V.; Tully, J. C. *J. Chem. Theory Comput.* **2006**, *2*, 229−235.
(66) Evans, D. J.; Hoover, W. G.; Failor, B. H.; Moran, B.; Ladd, A. J. C. *Phys. Chem. Chem. Phys.* **1983**, *28*, 1016−1021.
(67) García-Amorós, J.; Velasco, D. *Beilstein J. Org. Chem.* **2012**, *8*, 1003−1017.
(68) Yager, K. G.; Barrett, C. J. In *Smart Light-Responsive Materials:Azobenzene-Containing Polymers and Liquid Crystals*; Zhao, Y., Ikeda, T., Eds.; John Wiley & Sons, Inc.: New York, 2009; pp 1−27.
(69) Weingart, O.; Koslowski, A.; Thiel, W. *J. Chem. Theory Comput.* **2012**, *8*, 2352−2358.
(70) Arenas, J. F.; Tocon, I.; Otero, J. C.; Marcos, J. *J. Mol. Struct.* **1995**, *349*, 29−32.
(71) Arenas, J. F.; Tocon, I. L.; Otero, J. C.; Marcos, J. I. *J. Phys. Chem.* **1995**, *99*, 11392−11398.
(72) Choi, C. H.; Kertesz, M. *J. Phys. Chem.* **1997**, *101*, 3823−3831.
(73) Matousek, P.; Parker, A. W.; Phillips, D. *Chem. Phys. Lett.* **1997**, *278*, 56−62.
(74) Dobryakov, A. L.; Ioffe, I.; Granovsky, A. A.; Ernsting, N. P.; Kovalenko, S. A. *J. Chem. Phys.* **2012**, *137*, 244505.
(75) Myers, A. B.; Mathies, R. A. *J. Chem. Phys.* **1984**, *81*, 1552.
(76) Stuart, C. M.; Frontiera, R. R.; Mathies, R. A. *J. Phys. Chem. A* **2007**, *111*, 12072−80.